SYNTHESIS, STRUCTURE, AND ANTIMICROBAL ACTIVITY OF A SERIES OF NOVEL HETEROCYCLIC AZO-COLORANTS DERIVED FROM α-DICARBONYL COMPOUNDS

Thi Ngoc Anh Vu[1,2], Nadezhda Polyanskaya[3,4,5], Svetlana Bozhenkova[4], Viktor Khrustalev[3,6], Andrey Utenyshev[4,7], Anton Shetnev[8], Igor Filenko[9], Minh Chin Huynh[10], Anh Nguyen Van[11], Olga Kovalchukova[3,4]

[1] *Laboratory of Advanced Materials Chemistry , Institute for Advanced Study in Technology, Ton Duc Thang University, Ho Chi Minh City, Vietnam*

[2] *Faculty of Applied Sciences, Ton Duc Thang University, Ho Chi Minh City, Viet Nam*

[3] *Peoples' Friendship University of Russia (RUDN University), 6, Miklukho-Maklaya Str., Moscow 117197, Russia*

[4] *A.N. Kosygin Russian State University, 1-3, Malaya Kaluzhskaya Str., Moscow 117997, Russia*

[5] *Petrovsky Medical University, 3, Tsuriupy Str., Moscow 117418, Russia*

[6] *Zelinsky Institute of Organic Chemistry of RAS, 47 Leninsky Prospect, 119991 Moscow, Russian Federation*

[7] *Federal Research Center of Problem of Chemical Physics and Medicinal Chemistry RAS, 1, Academician Semenov Avenue, Chernogolovka, Moscow Region, 142432, Russia*

[8] *Yaroslavl State Pedagogical University named after K.D.Ushinsky, 108, Respublikanskaya Str., Yaroslavl, 150000, Russia*

[9] *Russian Institute for Scientific and Technical Information (VINITI RAS), 20, Usievich Str., Moscow, 125315, Russia*

[10] *Ho Chi Minh City Department of Health, Ho Chi Minh City, 700000, Vietnam.*

[11] *Faculty of Food Science and Technology, Ho Chi Minh City University of Industry and Trade , Ho Chi Minh City, 700000, Vietnam*

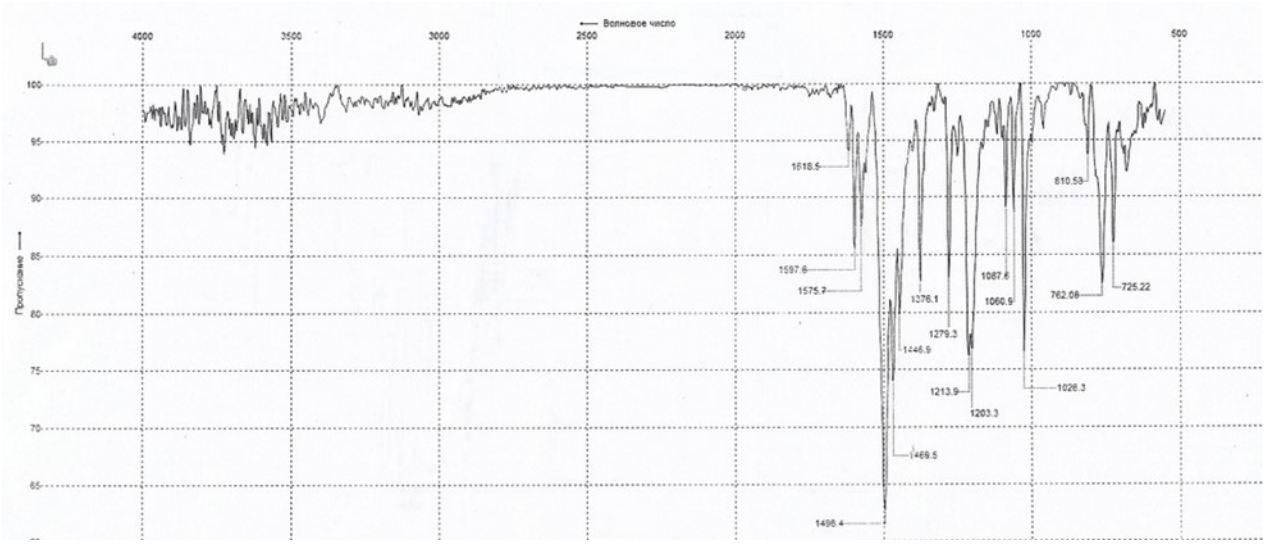

Fig 1S. IR Spectrum of L^1

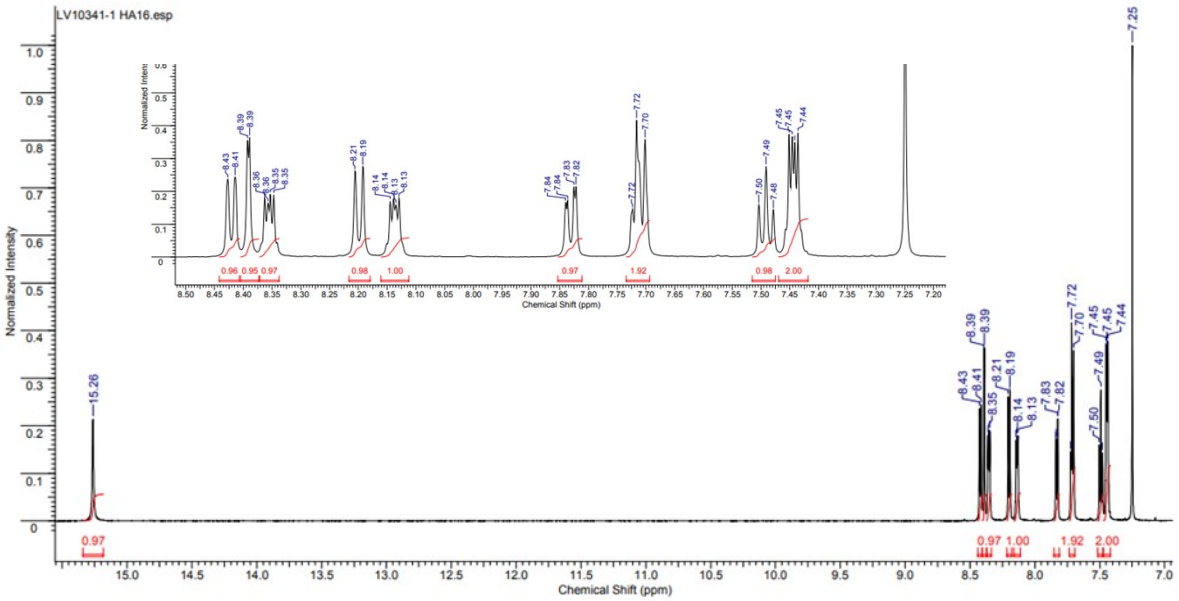

Fig 2S. ^{1}H NMR spectrum of L^1

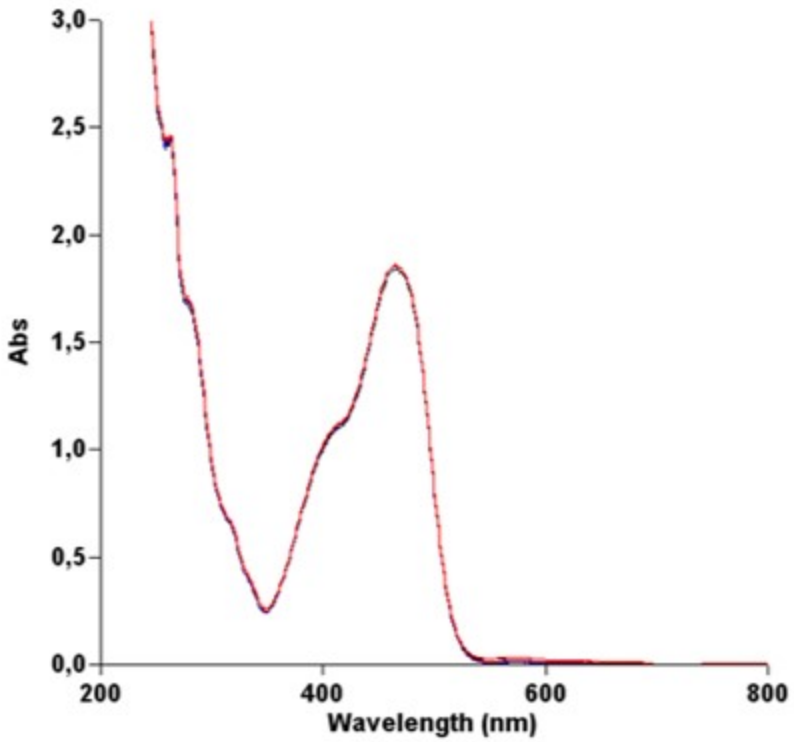

Fig 3S. UV-Vis spectrum of L^1 in ethanol

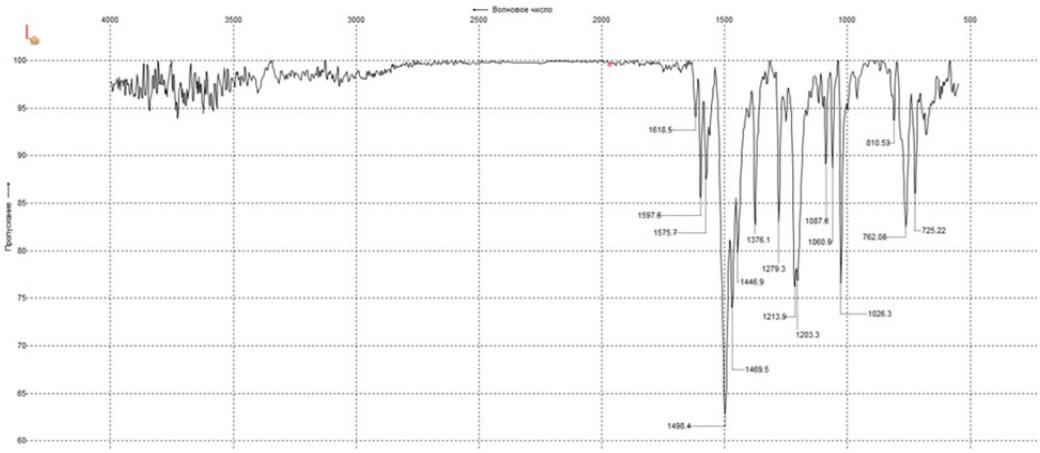

Fig 4. IR spectrum of L^3

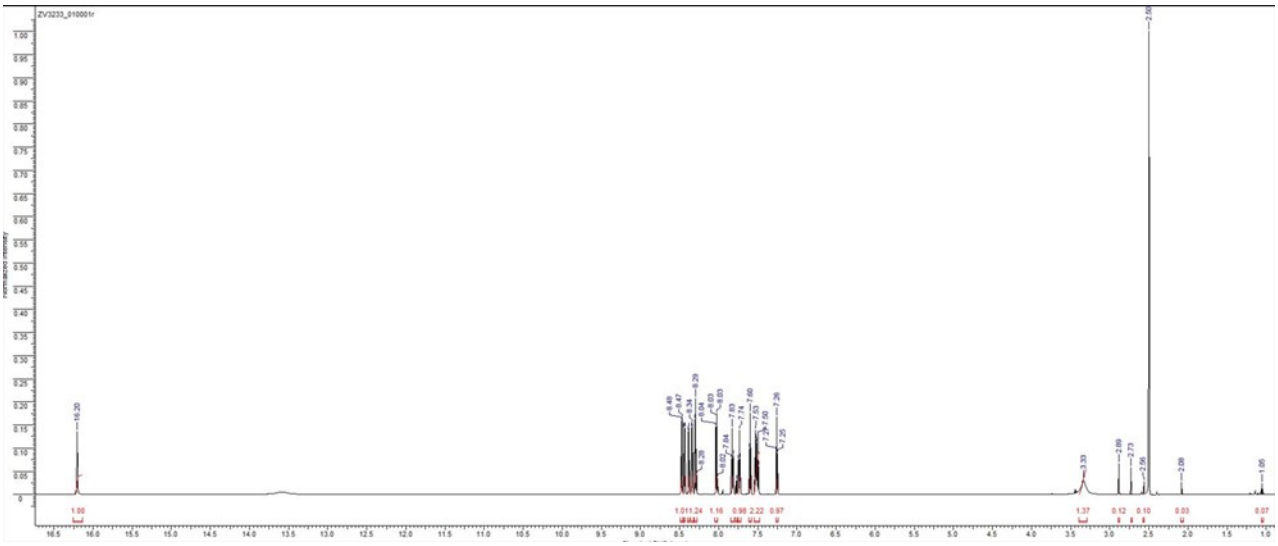

Fig 5. ^{1}H NMR spectrum of L^{4}

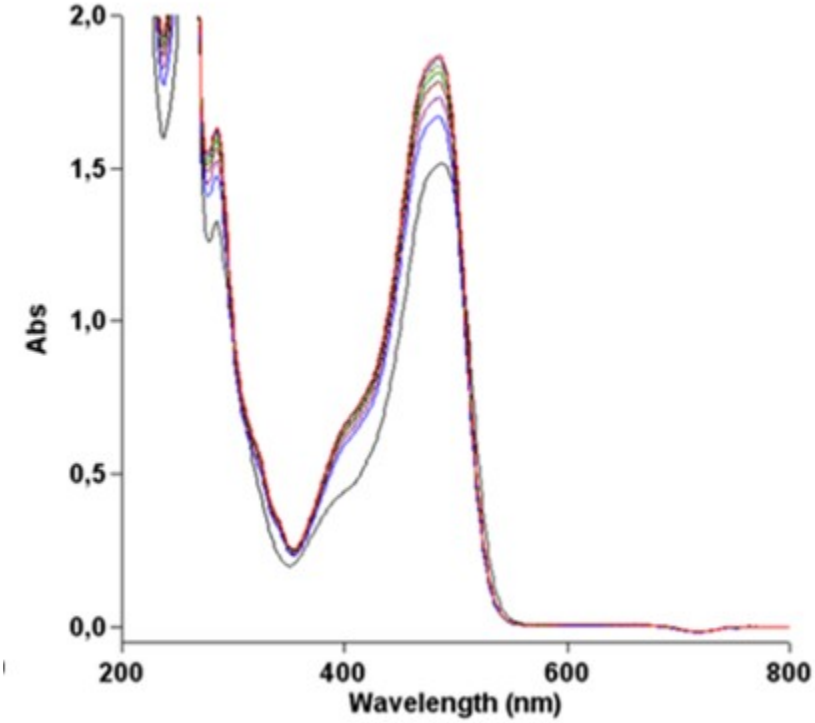

Fig 6: UV-Vis spectrum of L^{3}

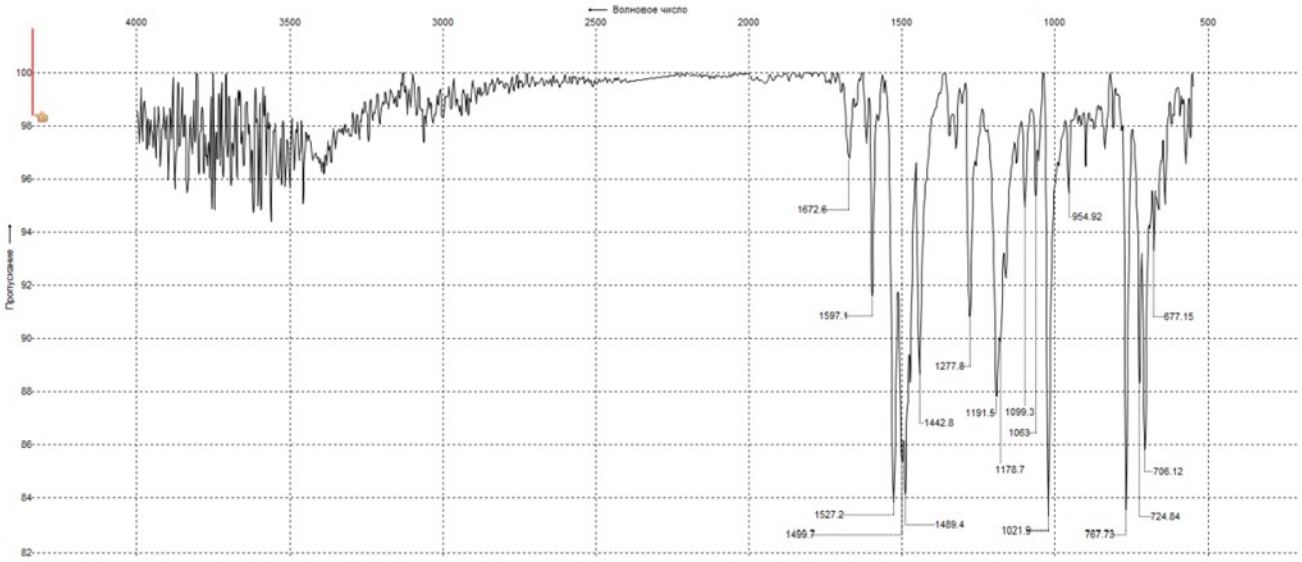

Fig 7S. IR spectrum of L^4

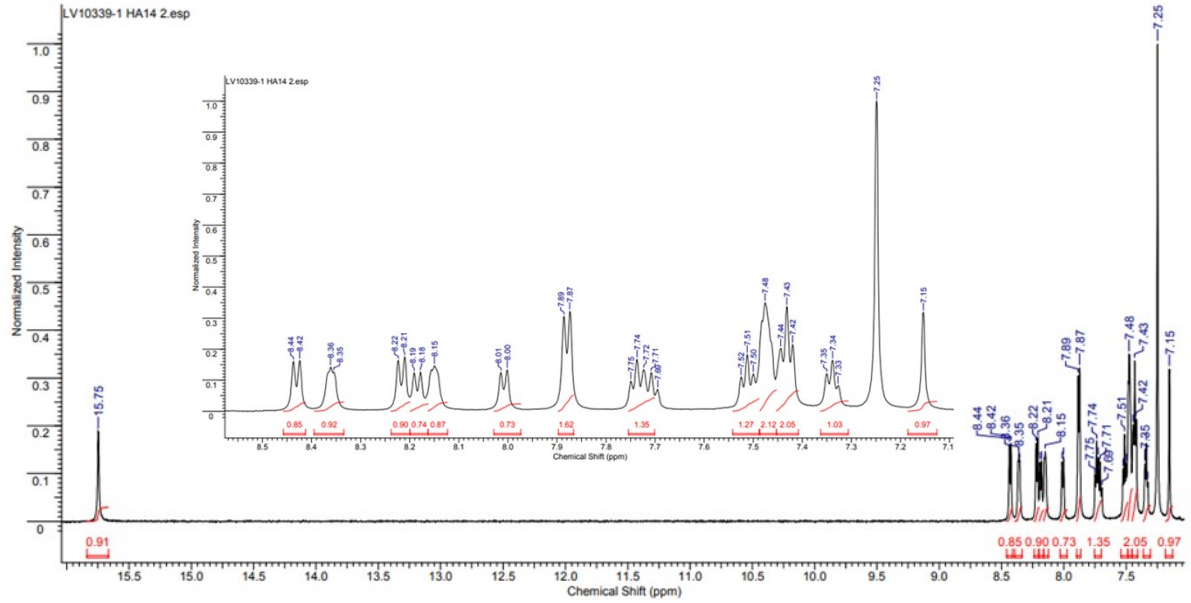

Fig 8S. ^{1}H NMR spectrum of L^4

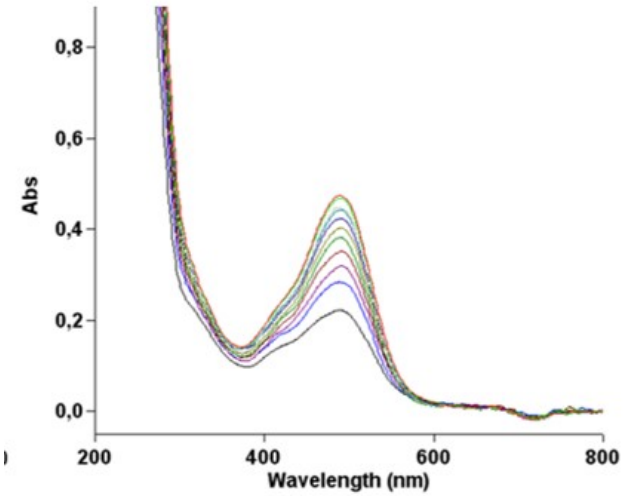

Fig 9S. UV-Vis spectrum of L^4

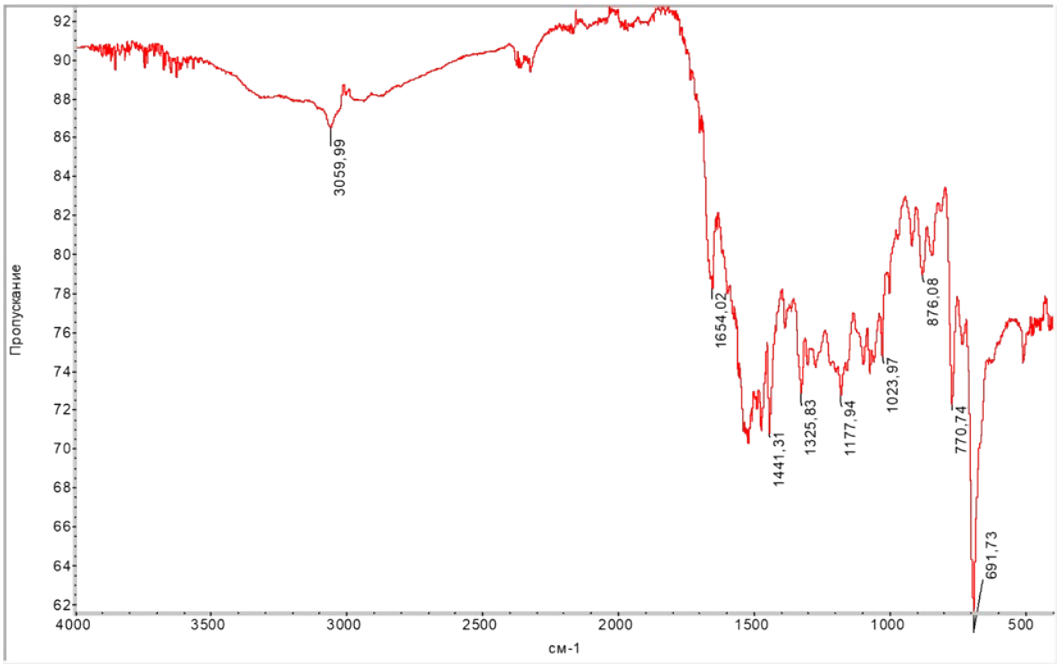

Fig 10S. IR spectrum of L^5

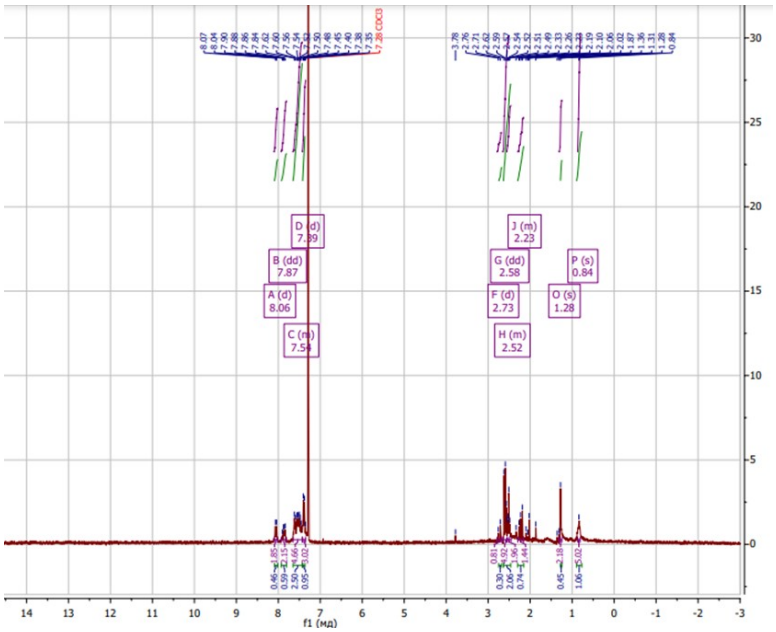

Fig 11S. ^{1}H NMR spectrum of L^{5}

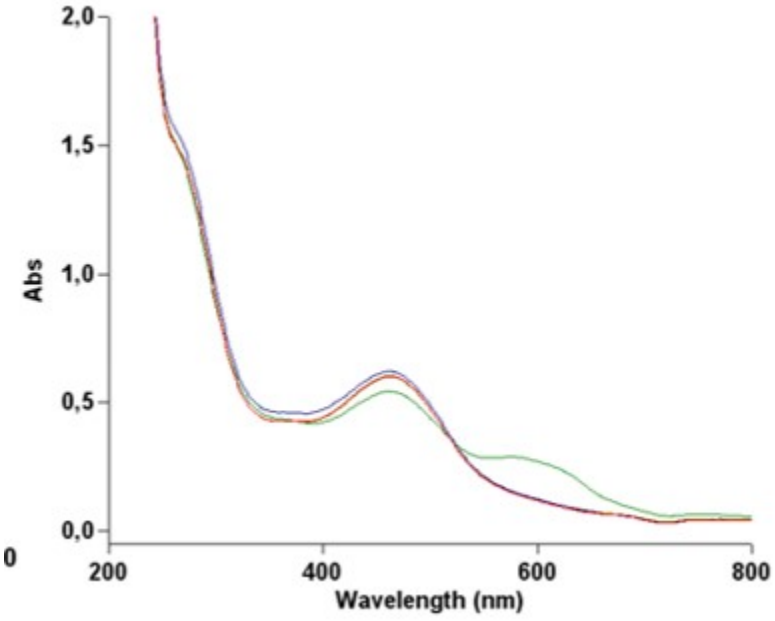

Fig 12S. UV-Vis spectrum of L^{5}

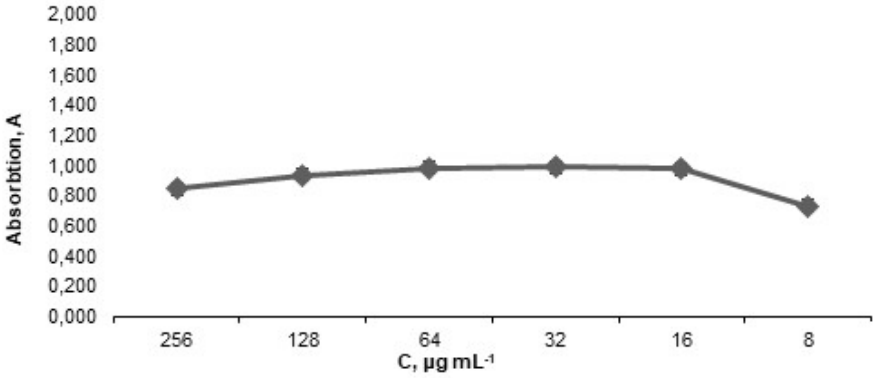

Figure 13S. Change in absorption when L^1 is exposed to the *Escherichia coli C1* strain at concentrations of 8-256 μg mL^{-1} (example of an inactive compound).

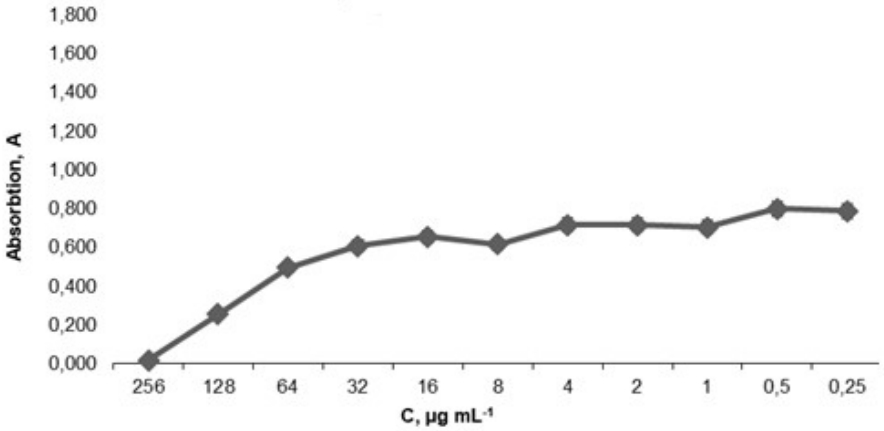

Figure 14S. Change in absorption when L^3 is exposed to the *Escherichia coli C1* strain at concentrations of 0,25-256 μg mL^{-1} (example of an active compound).

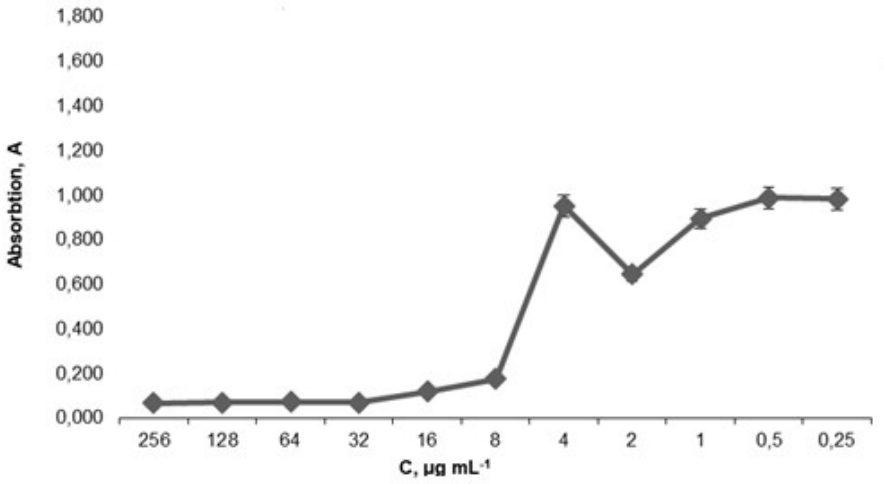

Figure 15S. Change in absorption when L^4 is exposed to the *Staphylococcus aureus ATCC-25923* strain at concentrations of 0,25-256 μg mL^{-1} (example of an active compound).

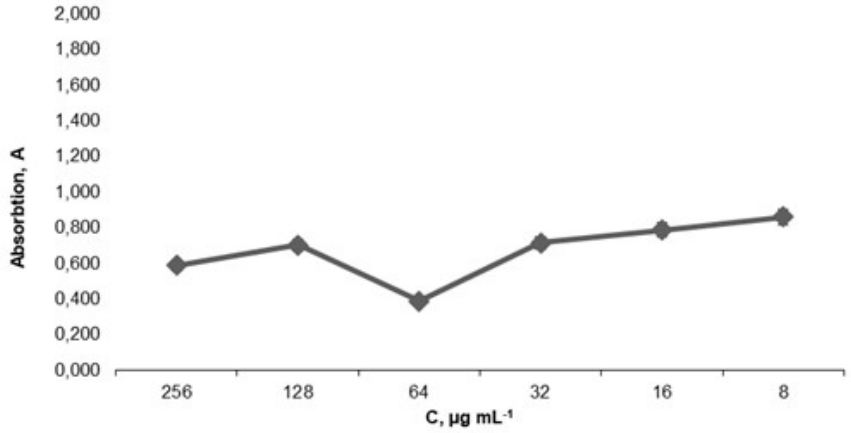

Figure 16S. Change in absorption when L^1 is exposed to the *Staphylococcus aureus ATCC-25923* strain at concentrations of 8-256 μg mL^{-1} (example of an inactive compound).

Ligand L^3	
5V8E (*B. cereus*)	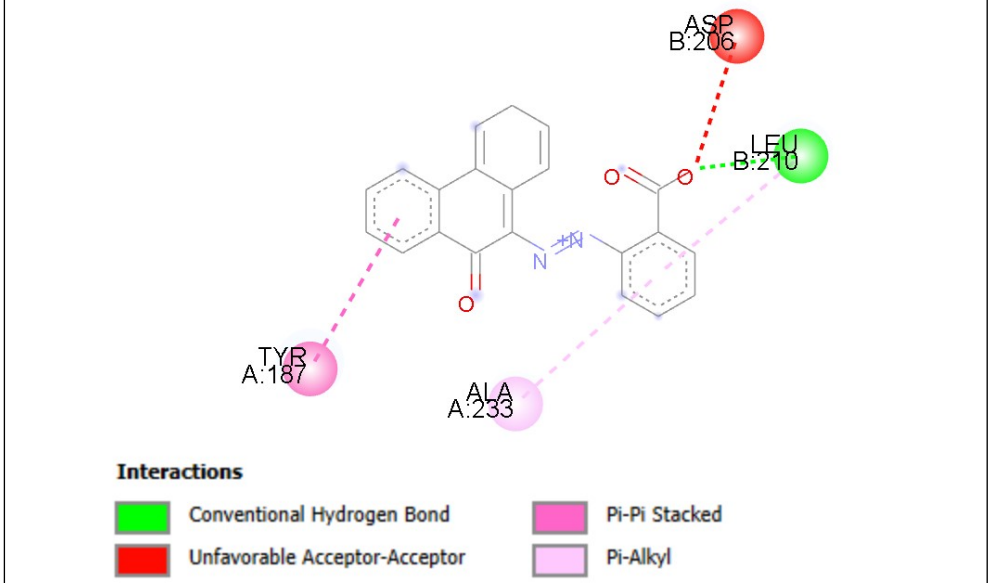

2BL8 *(E. faecium)*	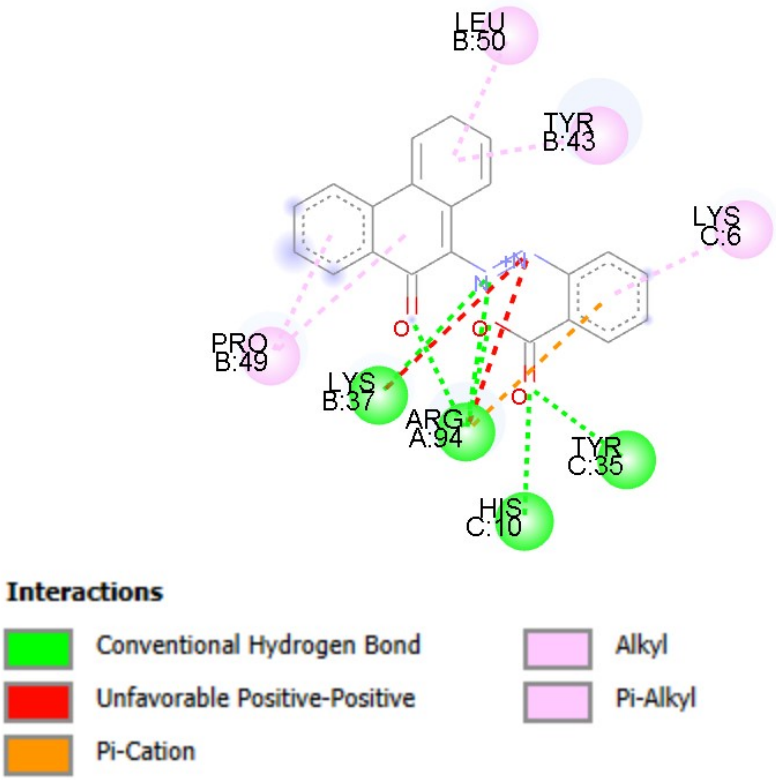
4PRV *(E. coli)*	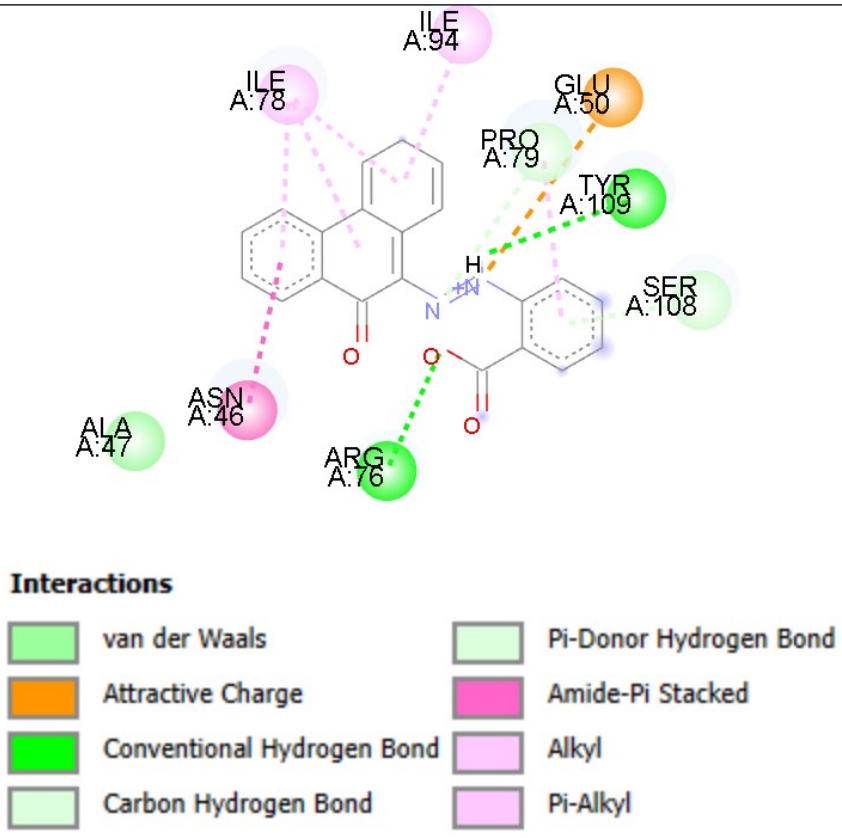

1JIL *(S. aureus)*	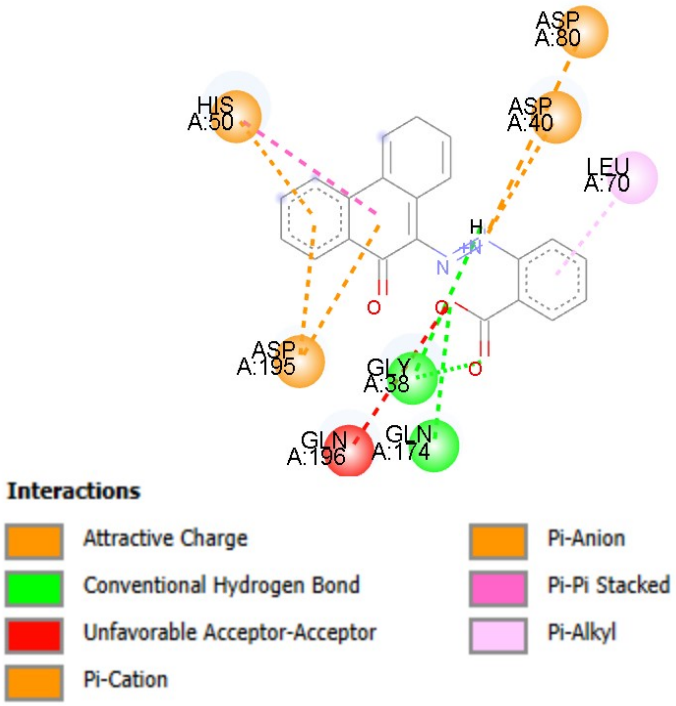
1GWE *(M. luteus)*	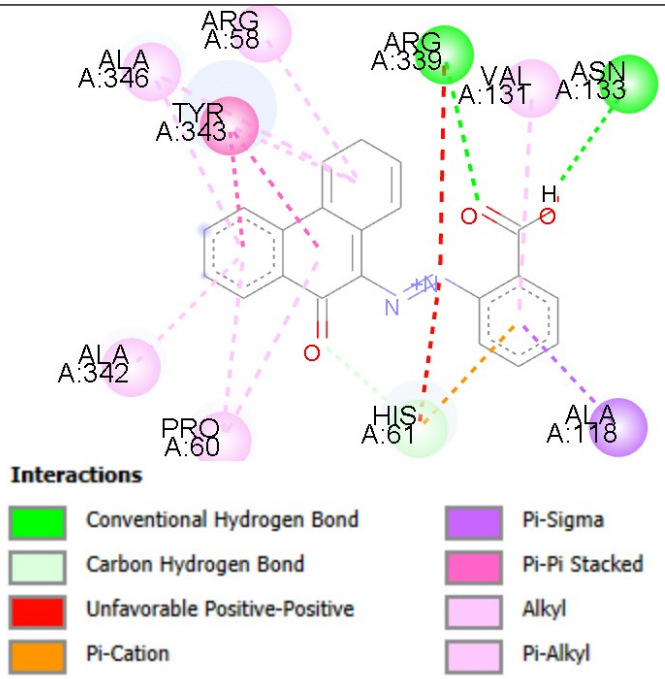

5V00 *(P. fluorescens)*	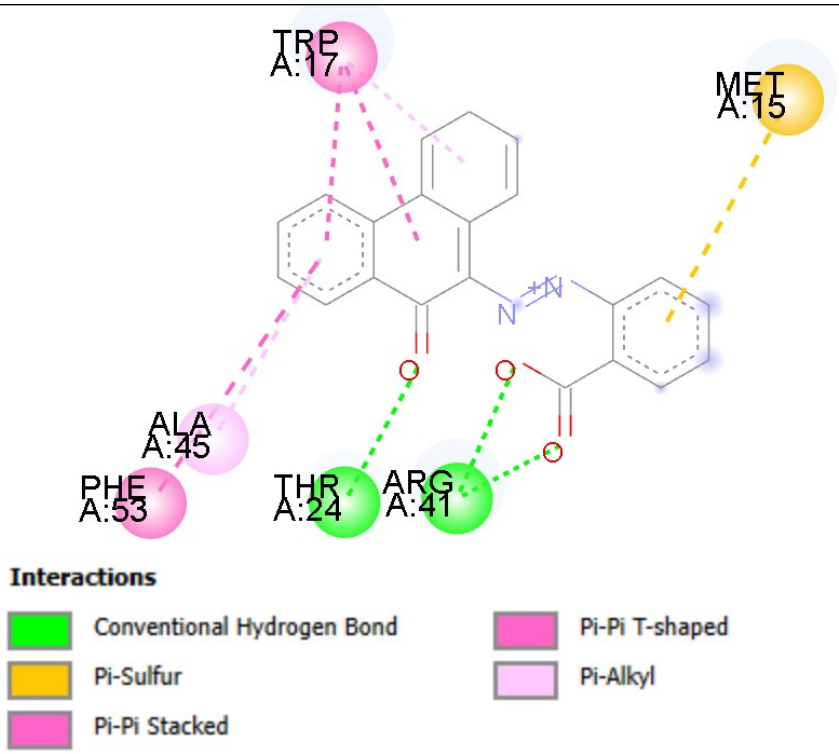
L[4]	
5V8E (*B. cereus*)	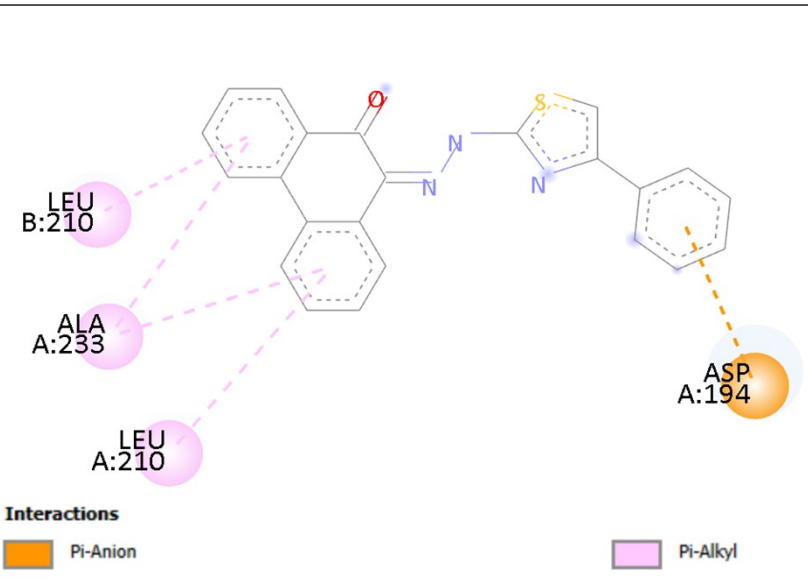

2BL8 *(E. faecium)*	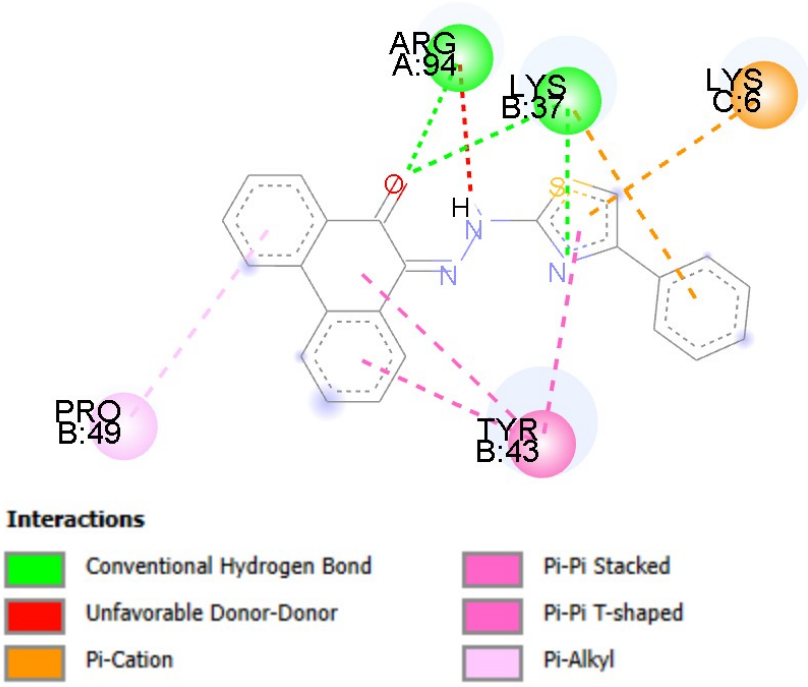
4PRV *(E. coli)*	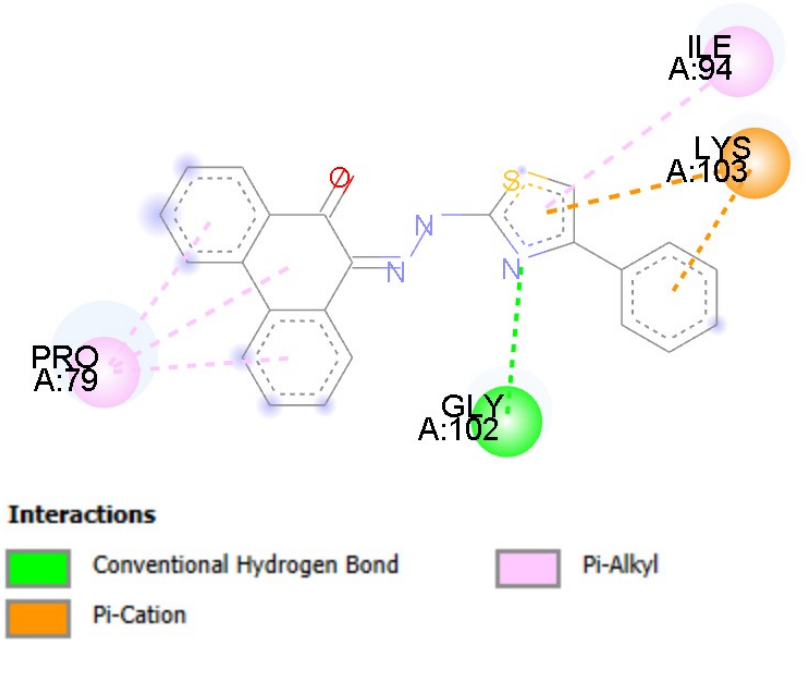

1JIL *(S. aureus)*	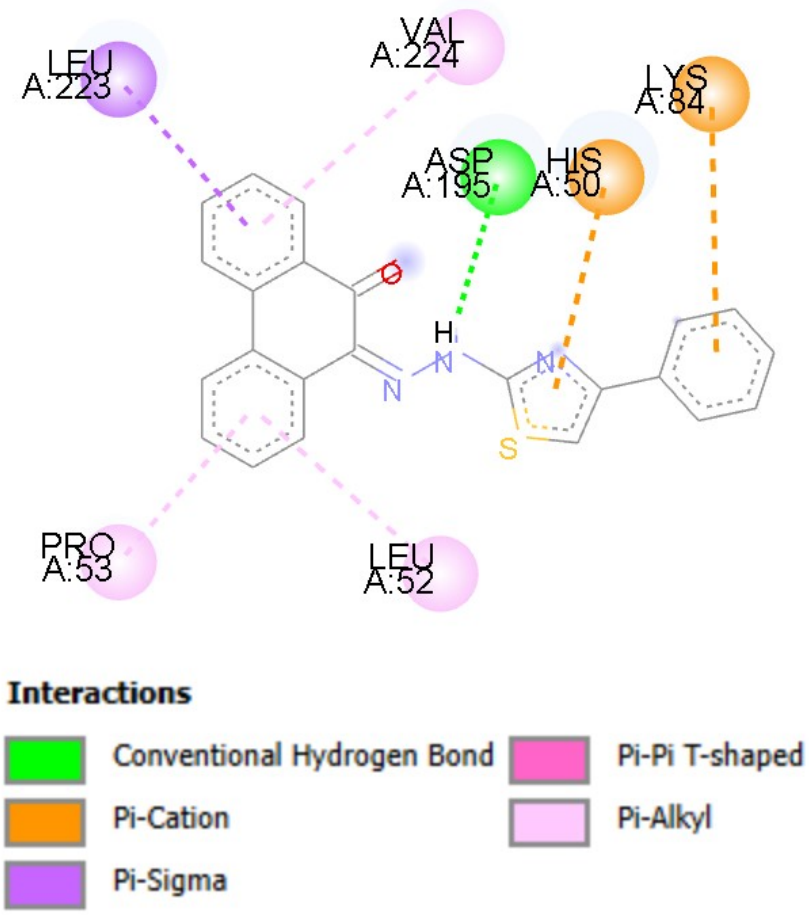

1GWE *(M. luteus)*	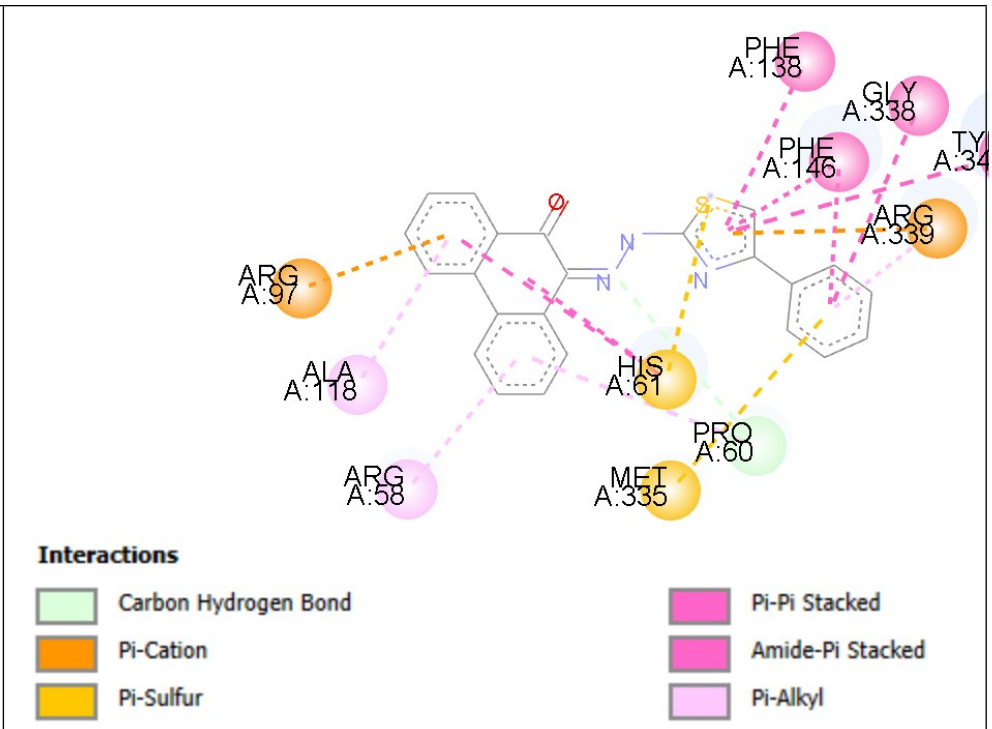
5V00 *(P. fluorescens)*	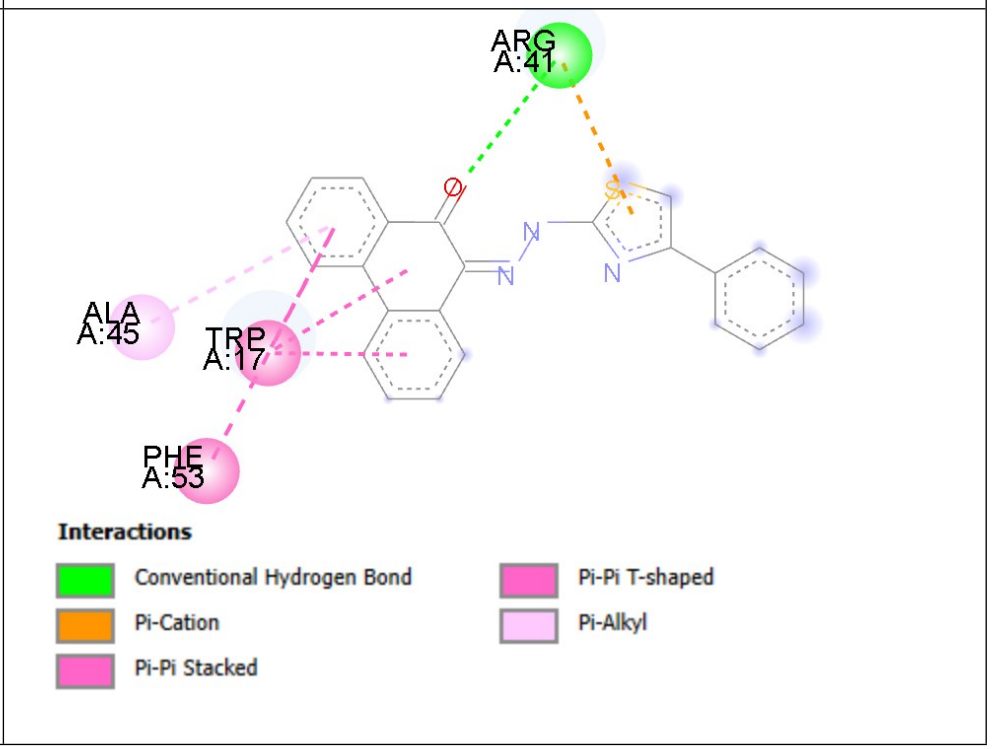

Figure 17S. 2D Chemical Structures representing protein-ligand interactions of L^3 and L^4

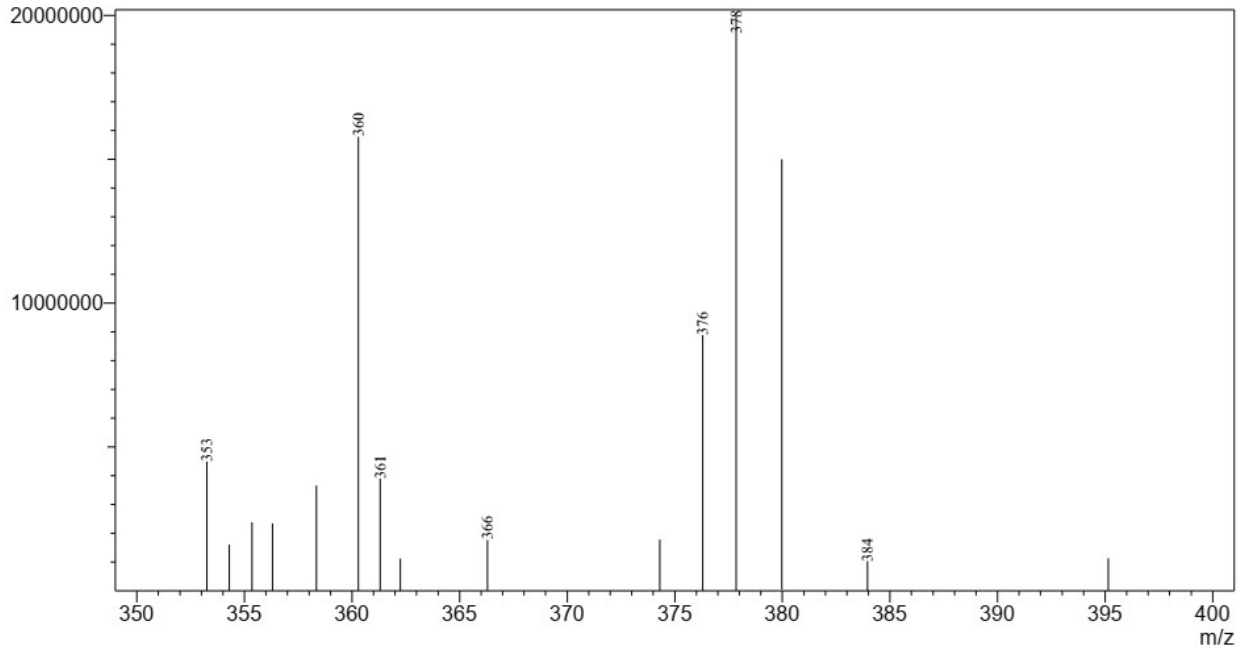

Fig 18S. Mass spectrum of L^1

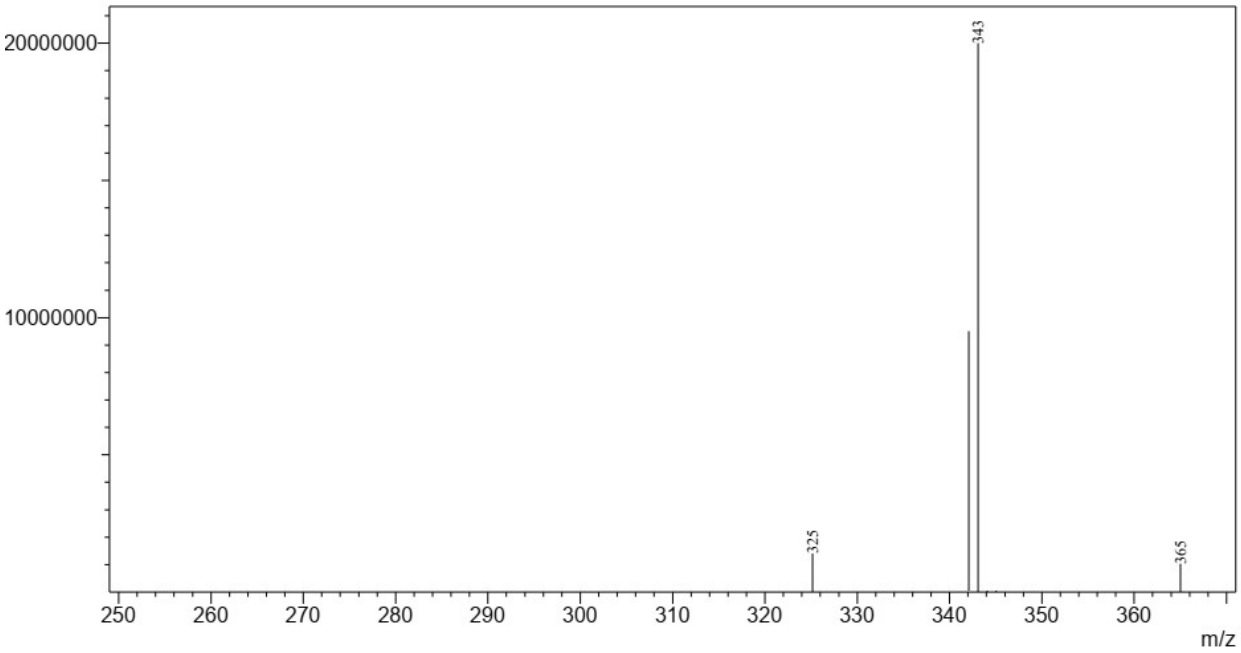

Fig 19S. Mass spectrum of L^3

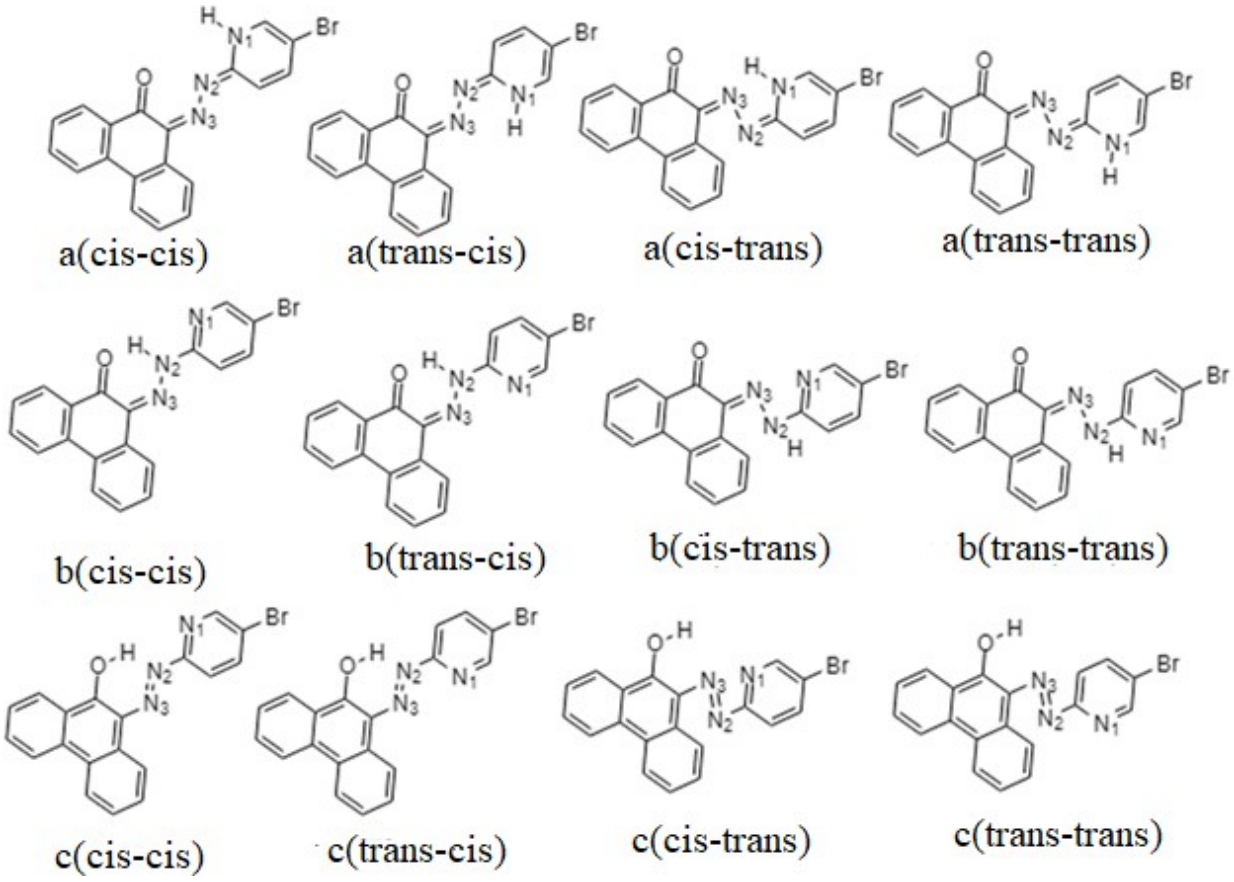

Figure 20S. Possible tautomeric forms of L^1

Table 1S. Relative energies (kJ/mole) of cis-isomers of zwitter-ionic (a), hydrazo (b) and azo (c) forms of L^1-L^6 according to DFT calculations.

Tautomer	Compound	L^1	L^2	L^3	L^4	L^5	L^6
a		96.5	86.34	_	70.86	47.47	221.01
b		0	0	0	0	9.04	0
c		33.8	0	31.44	24.14	0	12.51

Table 2S. Hemolytic activity of L^3 and L^4.

Compound	HC_{50}, μg mL^{-1} RBC
L^3	>32
L^4	>32

Table 3S. The crystal data and structure refinement of L^2 and L^4.

Compound	L^2	L^4
Empirical formula	$C_{18}H_{11}ClN_4O$	$C_{23}H_{15}N_3OS$
Formula weight	334.76	381.44
T(K)	100(2)	100(2)
λ (Å)	1.54184	1.54184
Crystal system	orthorhombic	monoclinic
Space group	*P*na2_1	*P*2_1/c
Unit cell dimensions:		
a, Å	16.4130(11)	20.2762(5)
b, Å	22.3174(14)	5.30357(13)
c, Å	3.9518(2)	16.5308(4)
α, deg.	90	90
β, deg.	90	104.649(2)
γ, deg.	90	90
V, $Å^3$	1447.53(15)	1719.87(7)
Z	4	4
D_{calc} (g cm^{-3})	1.536	1.473
Absorption coefficient, μ, mm^{-1}	2.449	1.830
F(000)	688	792
Crystal shape	needle	plate
Crystal color	light-yellow	dark-red
Crystal size, mm	0.53×0.04×0.02	0.12×0.12×0.02
Theta range for data collection	3.343–79.337	2.252–80.128
Index ranges	$-20 \le h \le 19$;	$-25 \le h \le 24$;

	$-28 \leq k \leq 24$;	$-6 \leq k \leq 6$;
	$-4 \leq l \leq 5$	$-21 \leq l \leq 20$
Reflections collected	10280	41624
Independent reflections	2709	3593
Reflections collected with $I > 2\sigma(I)$	2249	3412
Absorption correction	Gaussian	Multi-scan
T_{min} / T_{max}	0.392 / 1.000	0.575 / 1.000
Data / restraints / parameters	2709 / 1 / 220	3593 / 0 / 258
Goodness-of-fit (GOF) on F^2	1.033	1.020
R_1 [$I > 2\sigma(I)$]	0.0836	0.1020
wR_2 [all data]	0.2133	0.2271
Largest dif. peak and hole	1.195 / -0.707	0.914 / -0.693
CCDC No	2482127	2482128